C_{60}^- thermal electron-emission rate

K. Hansen *

Center for Joint Quantum Studies and Department of Physics, School of Science, Tianjin University, 92 Weijin Road, Tianjin 300072, China

(Received 21 June 2020; accepted 4 November 2020; published 23 November 2020)

The thermal electron-emission rate constant for C_{60}^- has been deduced for internal energies from 9.7 to 14.1 eV from storage ring measurements of the decays of ions reheated with single-photon absorption. The thermal radiation from the ions is quantified from the data with respect to continuous cooling and discrete photon quenching.

DOI: 10.1103/PhysRevA.102.052823

I. INTRODUCTION

Measurements of rate constants in molecular beams with standard approaches require very good control over the excitation energy. A width in the internal energy distribution in a decaying particle or molecule will also introduce a width in the distribution of rate constants in the beam molecules, and due to the strong dependence of rate constants on excitation energy, any spread in energy is strongly amplified for the rate constants. This makes direct measurement of rate constants very difficult, even for relatively narrow internal energy distributions. The problem is not solved by extracting molecules from canonical thermal distributions into molecular beams, as demonstrated in Ref. [1] with a calculation of a numerical example for C_{60}^-.

The detrimental consequence of a finite width of the internal energy distribution to a simpleminded determination of rate constants is perhaps best demonstrated by considering the measured decay rates vs the rate constants present in the ensemble. Allowing for measurements over all possible timescales, an Arrhenius-type analysis would be based on the approximation

$$k(\langle E\rangle) \stackrel{?}{\approx} \langle k(E)\rangle, \tag{1}$$

where the average is over the energy distribution. This is emphatically wrong. Adding a finite dynamic time range to the measurement of the right-hand side will make this poor approximation even worse.

In fact, when the energy distribution of the molecules in a beam is sufficiently broad and in the absence of competing channels, molecular decay will occur with a rate with a time dependence close to $1/t$ [2]. In the presence of the frequently occurring phenomenon of thermal radiation, this power law will be suppressed at long times with an almost exponential time dependence [3].

Situations with broad energy distributions are seen for all particle sizes but arise particular frequently for large molecules and clusters because, for these, excitation to internal energies where reactions occur on measurable timescales will require large amounts of energy, up to several tens of eV. Deposition of precise amounts of energies of such magnitudes is a very challenging experimental task. Photoexcitation experiments with a single high-energy photon, for example, will often lead to direct (first or secondary) ionization of the molecules or to electron detachment from anions. The alternative strategy of multiple absorption of smaller energy photons suffers from the inherent spreads in absorption statistics. Collisional excitation is possible, as demonstrated with electron collisions with fullerenes [4,5], but these suffer from a broad energy transfer efficiency, requiring a detailed quantitative analysis of the reaction products with a number of highly nontrivial assumptions.

The origin of the power-law behavior is the loss of a well-defined energy scale in the excitation energy distribution caused either by such postproduction excitation or by the use of hot sources, which almost unavoidably produce clusters with broad energy distributions. For a unimolecular decay in vacuum, loss of an energy scale is equivalent to loss of a timescale. This is reflected in the absence of a characteristic timescale in the $1/t$ dependence of the decay rate.

If one wants to measure absolute energies under such conditions, it is therefore necessary to introduce an energy scale by hand. Doing so, it turns out that such a procedure allows us to determine the rate constant also for these broad energy distributions. The demonstration of this procedure is the purpose of this article.

The reheating experiments that provide the data for the analysis here were obtained with C_{60}^- in the experiments reported in Ref. [6]. In these experiments, the anions were created hot from the source and injected into an electrostatic storage ring, where they decayed by spontaneous electron emission. At a variable time after production, a small fraction of the un-decayed ions were reheated by one-photon excitation. The photon energy absorbed and dissipated caused a heating of the molecule that led to an enhanced delayed thermal electron emission. The time profile of the enhanced decay was used to locate the equivalent backshifted time, i.e., the time where the spontaneously decaying ions decayed with the same time dependence as the laser excited ions. An overall multiplicative constant on the enhanced decay, which reflects quantities such as laser fluence, beam overlap, and photon

*klavshansen@tju.edu.cn

absorption cross section was only relevant for the amplitude of the laser-enhanced signal and did not enter the analysis.

Together with the instrumental laser firing time, the determination of this apparent shift of the zero time of the power-law decay due to the reheating provides the time interval during which one photon energy was lost. The procedure can therefore be used to determine the absolute cooling rate of the ions. The results obtained were in very good agreement with the known facts of C_{60}^-, such as the electron affinity, and also with the model for the radiative cooling developed in Ref. [7].

The data from this experiment somewhat surprisingly also allow for the determination of the parameters that determine the energy resolved rate constants. Furthermore, they provide a measure of the relative importance of continuous and discrete cooling. These two types of thermal photon emission differ only by the magnitude of the energies of the photons emitted, and thereby by the effect they have on the measured decay dynamics of the ions.

The outcome of the analysis of the C_{60}^- data will provide the absolute decay rate, parametrized by the product of activation energy and heat capacity, the frequency factor of the rate constant, and a binary spectral distribution of the thermally emitted photons, all pertaining to the excitation energy interval between 9.7 and 14.1 eV.

The remainder of the paper is divided into a section where the theory behind the experimental data and the present analysis is described in some detail. This is followed by a section where the experiments are described, after which a section presents the data analysis and the results. Finally, the procedure and the results are summarized and discussed.

II. THEORETICAL BACKGROUND

The spontaneous statistical decay rate of an ensemble of particles in a molecular beam is given by the decay rate constant averaged over all excitation energies present in the ensemble [1,3]:

$$R(t) \propto \int_0^\infty g(E)k(E)\exp\left[-k(E)t\right]dE. \tag{2}$$

where R is the measured decay rate, i.e., the number of decays per time unit, and $k(E)$ is the decay rate constant of an ion with excitation energy E. The decay rate on the left-hand side of Eq. (2) is not any proxy for a rate constant, it should be emphasized. Decays of systems with a specific energy remain exponential, as the equation also assumes. The quantity $g(E)$ is the ensemble density of excitation energy at the time it was created in the source, and t is the time elapsed from the creation of g in the source to the measurement. The constant of proportionality is the combined transmission and detection efficiency. When $g(E)$ is broad, the integrand peaks at the rate constant k_m for which

$$\frac{d}{dE}k_m(E)\exp\left[-k_m(E)t\right] = 0 \Rightarrow k_m(E)t = 1, \tag{3}$$

corresponding to a peak value of $\exp(-1)/t$ for $k(E)\exp[-k(E)t]$. This result is derived without specifying the expression for $k(E)$ and holds generally, insofar as Eq. (3) has solutions, which may not be the case for ultrafast processes but will be the case for measurement times relevant here. Implicit in the calculation is the assumption that the decay process involves an activation energy, and the obvious requirement that it is observable, i.e., leads to a change in mass or charge state. The equation only has one solution if $k(E)$ is a monotonically increasing function of E, which can also be safely assumed here, but which might not be true around a phase transition.

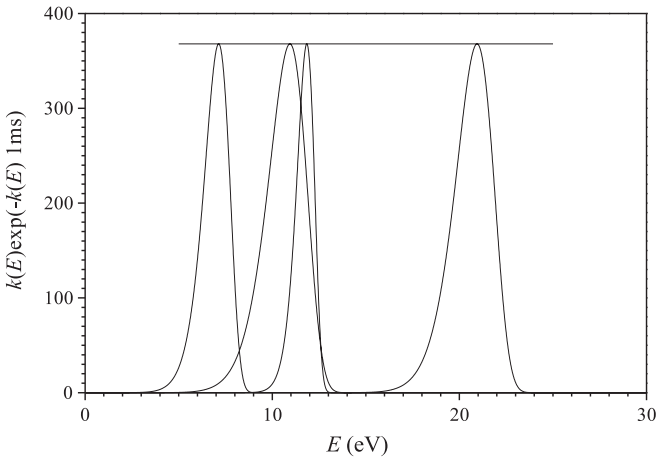

FIG. 1. The product of rate constants and survival probability for a broad energy distribution after 1 ms for a few different parameters for the rate constant given in the main text. The line is the calculated value of $1000/\exp(1)$ s^{-1}. The parameters are, from low to high peak energies: $(\omega, \phi C_v, E') = (10^{14}$ Hz, 434 eV, 10 eV), $(10^{12}$ Hz, 434 eV, 10 eV), $(10^{14}$ Hz, 300 eV, 0), and $(10^{12}$ Hz, 434 eV, 0).

It is worth demonstrating the generality of the result in Eq. (3) with some different expressions for rate constants. Figure 1 shows a few examples. The expression for the decay constant, which will also be used in the analysis, is of the simple form

$$k = \omega\exp\left(-\frac{\phi C_v}{E+E'}\right). \tag{4}$$

Here C_v is the canonical heat capacity in units of k_B, less one due to the microcanonical correction [8] ($k_B = 1$ will be used throughout), and ϕ is the decay channel activation energy. The parameter ω plays the same role as the frequency factor in the canonical Arrhenius expression, although the two numerical values are in general different. The energy E' is the offset in the caloric curve, $E = C_vT + E'$, which cannot be assumed zero. For thermionic emission from C_{60}^-, the parameter ϕ is to a first approximation expected to be the electron affinity of 2.67–2.68 eV [9,10]. In spite of its simplicity, Eq. (4) is very accurate for our purpose because only an energy interval of ca. 4 eV is covered in the experiments here. This question is discussed in the Appendix and corrections to parameters made in the discussion section.

The rate constants used in Fig. 1 are all variations of the rate constant in Eq. (4). Other examples with different functional forms are given in Ref. [3], with an identical conclusion concerning the peak values.

The decay rate is the integral of the peaks in Fig. 1. The integral is on the order of the width times the height. The order

of magnitude of the widths of the peaks, δE, is given by

$$\frac{d\ln(e^{-kt})}{dE}\delta E \approx 1 \Rightarrow \delta E \sim \left(\frac{d\ln k}{dE}\right)^{-1}, \tag{5}$$

where $k = 1/t$ was used. Given the rapid variation of k with energy, this will remain fairly constant over a wide range of times. This suggests the possibility that also the decay rate may vary approximately as $1/t$. To examine this question the decay rate is calculated by considering the time dependence of the energy distributions. Ignoring the variation of g with energy, the energy distribution of the surviving ions, $\exp[-k(E)t]$, is essentially constant up to an energy close to the value defined by $k(E) = 1/t$, at which point it bends over and rapidly approaches zero. The motion of this crossover energy with time represents the decay rate. Solving Eq. (4) for E and differentiating with respect to time then gives the decay rate:

$$R(t) = -c'g\frac{dE(k=1/t)}{dt} = c'g\frac{\phi C_v}{[\ln(\omega t)]^2}\frac{1}{t}, \tag{6}$$

where c' is a constant that includes the detection, transmission efficiency, and other instrumental parameters, and $g(E)$ is set to a constant, $g = g(E(k = 1/t))$. Absorbing g into the constant, $c \equiv c'g$, and rewriting gives

$$\frac{1}{t} = k_m = R(t)\frac{[\ln(\omega t)]^2}{c\phi C_v}, \tag{7}$$

where k_m is the value for which the decay peaks. The difference between the time dependence of the decay rate and the rate constant at the peak decay rate is the time variation of the width of the decaying peak considered a function of excitation energy and is summarized by the factor $[\ln(\omega t)]^2$. This equation has been established previously; see, e.g., Ref. [3] and references therein, and has been used to determine heat capacities of water clusters and radiative cooling of cationic carbon clusters experimentally, for example.

In the presence of thermal radiation, relevant for C_{60}^- in the experimental data used here, the relation must be reconsidered. In principle also the C_2 emission is a possible channel. However, this has an activation energy which is close to four times that of electron emission from the anion and can safely be ignored. The only channel competing with electron emission is therefore thermal radiation.

In the context of ensembles there are two categories of thermal radiation, defined by the magnitude of the energies of the emitted photons. When the emission is by sufficiently low energy photons, the radiation is effectively a continuous cooling. This means that the energy distribution shifts down with time similarly to the nonradiative situation, just faster. The shape of the crossover region of the energy distribution is virtually unchanged in this small photon energy limit. When only this type of radiation is present, its effect can be determined from the observed decay rate with an expression analogous to Eq. (7), where t' is given by

$$R(t) = \frac{cg\phi C_v}{t'\ln(\omega t')^2}, \tag{8}$$

from which the peak rate constant is identified as

$$k(t) = \frac{1}{t'}, \tag{9}$$

where t' is a fictitious time which is equal to the time needed to wait to have an identical decay rate in the absence of radiation. The decay at short times which is not influenced by any radiative cooling can be used to determine the constant of proportionality that links t and t'. In the logarithm the difference between the physical time and t' can often be ignored.

When high-energy photons are emitted, the simple power-law relation needs to be modified once more. Photon energies are considered large if the emission of a single photon will quench the decay on a timescale corresponding to the rate constant after emission. The precise energy where this shift from continuous cooling to quenching happens was analyzed in Ref. [11] and will be discussed here after the presence of these photons is quantified.

For the fullerenes, the largest part of the radiation is well understood as being carried by the broad surface-plasmon resonance [7]. Although centered at 20 eV, it reaches into the near infrared, which allows the low-energy tail to be excited thermally with an oscillator strength which gives a radiative energy emission rate which is two orders of magnitude higher than the contribution from the vibrational transitions [12]. The calculated magnitude is consistent with both the anion cooling and the original observation of the strong radiative cooling of the much hotter fullerene cation fragments [13]. The distribution of photon energies generated by the plasmon resonance emission covers both the small and large values, and both types of channels therefore need to be considered in the analysis.

Whereas for small photon energies the emitted power is the relevant quantity, for large photon energies it is the emission rate constant. Although photon emission rate constants vary with the temperature to the power six [12], this is still slow compared with the variation of the rate constant of the observed thermionic emission rate constant, and we can here set the discrete energy emission rate constant to a single value, k_p. Interestingly, the power of six which originates in a photon absorption cross section that varies with the square of the photon energy, has also been observed for larger, metallic nanoparticles [14,15]. The presence of high-energy photon radiation means that the abundances at the decaying edge, and hence also the decay rates, are reduced by the factor $\exp(-k_p t)$. Together with the effect of the continuous cooling and after normalization to the short time behavior of $1/t$, the observed rate R_n is then equal to

$$R_n(t) = \frac{1}{t'}e^{-k_p t} = k(t)e^{-k_p t}, \tag{10}$$

or

$$k(t) = R_n(t)e^{k_p t}, \tag{11}$$

where $k(t)$ is the thermionic rate constant at the peak of the energy distribution. The fitted curve from the experimentally measured spontaneous decay rate of C_{60}^- from the hot source used gives the function [6]

$$R_n(t) = \frac{1}{t}\exp(-122\mathrm{s}^{-1}t + 1320\mathrm{s}^{-2}t^2), \tag{12}$$

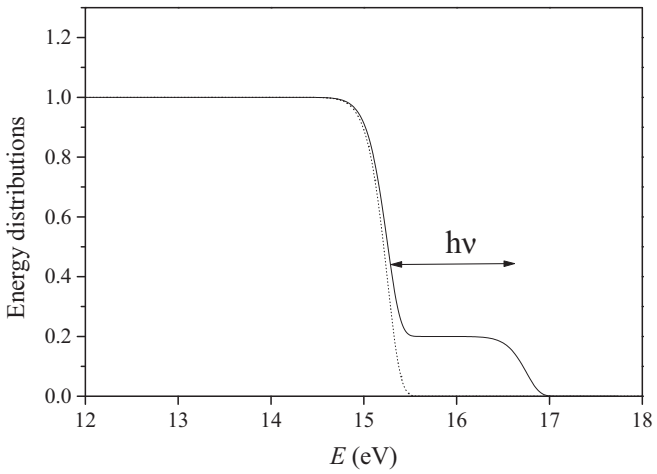

FIG. 2. A schematic view of the energy distributions immediately before (dotted line) and after (full line) a photon with energy $h\nu$ has been absorbed at t_{las}.

and hence

$$k(t) = \frac{e^{k_p t}}{t} \exp(-122\text{s}^{-1}t + 1320\text{s}^{-2}t^2). \quad (13)$$

The analysis so far has only dealt with the spontaneous decay. If the molecule is exposed to a laser pulse some time after production, the absorbing fraction of the energy distribution will be shifted up by the photon energy. The situation is illustrated schematically in Fig. 2. The small fraction of the distribution that has been shifted up in energy has almost the same shape as the unshifted distribution had at some earlier time, apart from the absolute height. This has been shown in Ref. [16] to which the reader is referred for details of the calculation. After photon absorption at t_{las} the decay rate is therefore given by

$$R_{las}(t) = pe^{-k_p(t_{las}-t_0)}R(t - t_{las} + t_0) + (1 - p)R(t), \quad (14)$$

where t_0 is a backshifted time, and p is the photon absorption probability. The spontaneous decay rate is a function of time and the physical interpretation of t_0 is that it is the time where the decay rate was equal to the rate observed after photon absorption. This time can therefore be determined by a fit of the first term on the right-hand side of Eq. (14) to the decay rate at earlier times. The fraction of absorbing ions, p, was so low in the experiments that it is practically unobservable in the second term in the equation. This facilitated the analysis although it is not an essential requirement. The nonzero value of k_p has no effect on this part of the analysis. It was not explicitly considered in Ref. [6], but the cooling rates obtained there remain unchanged, although it is clear that they only refer to the small photon energy cooling power.

The nonexponential decay is essential to determine the cooling with this procedure because, for nonexponential decays, the value of both p (or more precisely $pe^{-k_p(t_{las}-t_0)}$) and t_0 can both be determined, a possibility which is not present for an exponential decay.

As shown, decay rates are proportional to decay constants and Eq. (14) therefore also holds for the peak distribution values $k_m(t)$ with the substitution $R(t) \rightarrow k_m(t)e^{-k_p t}$. The values of t_0 depend on the photon energy and t_{las} but are independent of the absorption cross section and instrumental parameters. Keeping the laser firing time t_{las} fixed and varying the photon energy, it is therefore possible to obtain the variation of the rate constant with photon energy as

$$k_m(E(t_{las}) + h\nu) = e^{k_p t_0}R_n(t_0(t_{las}, h\nu)), \quad (15)$$

and similarly

$$k_m(E(t_{las})) = e^{k_p t_{las}}R_n(t_{las}). \quad (16)$$

The energy $E(t_{las})$ is the energy where the decay rate peaks at time t_{las}. It is unknown but both $h\nu$ and t_0 are known. As indicated in Eq. (15), the measured values of t_0 depend on both the laser firing time and the photon energy. When considering decay rates in the following, the term energy will always refer to this particular energy or the corresponding peak rate energy for the shifted distributions. In statements about the rate constant, the energy will refer to the argument in Eq. (4). Equations (15) and (16) are the basic equations for the analysis of the experimental data. They will be used below to express the ks in terms of known, experimental times and parameters of the decay. The subscript m indicates that the rate constant refers to a specific energy here. It will be dropped below.

It should be noted that, although a number of measured values of t_0 correspond to times before the mass selection has been completed in these experiments, this causes no problem for the analysis, because other experiments on C_{60}^- have established the short-time behavior as a well behaved power law, see e.g., [12], and this behavior is also well established as a general phenomenon, see, e.g., the examples listed in Ref. [3].

III. EXPERIMENTS

The data used for the analysis were recorded at the Tokyo Metropolitan University electrostatic storage ring, TMU e-ring. The analysis of the absolute cooling rates derived from these data was published in Ref. [6], and the description of the experiment here will be limited to the pertinent points. For a detailed description of electrostatic storage rings and their use for decay measurements, the reader is referred to the rich literature on the subject, see e.g., Refs. [17–22].

The C_{60}^- anions were produced in a laser ablation source without any cooling gas and injected into the ring together with some amount of other anionic carbon species produced during the ablation, mainly other fullerenes. The circulation time of C_{60}^- in the ring was 122 μs. A set of pulsed deflection plates was used to eject the unwanted species, based on their mass-dependent circulation time. This beam purification process was completed within 1 ms after production of the ions in the source.

After a variable storage time, the C_{60}^- beam was exposed to a laser pulse from a tunable optical parametric oscillator (OPO) laser, with photon energies which were varied between 1.9 and 2.7 eV in steps of 0.1 or 0.2 eV. Pulse energies were kept low, typically a few mJ or lower, to ensure single-photon absorption conditions. Spectra were recorded with laser firing times between 4 and 35 ms.

Figure 3 shows two example spectra that were recorded with laser firing time 12.5 ms and photon energies 2.0 and

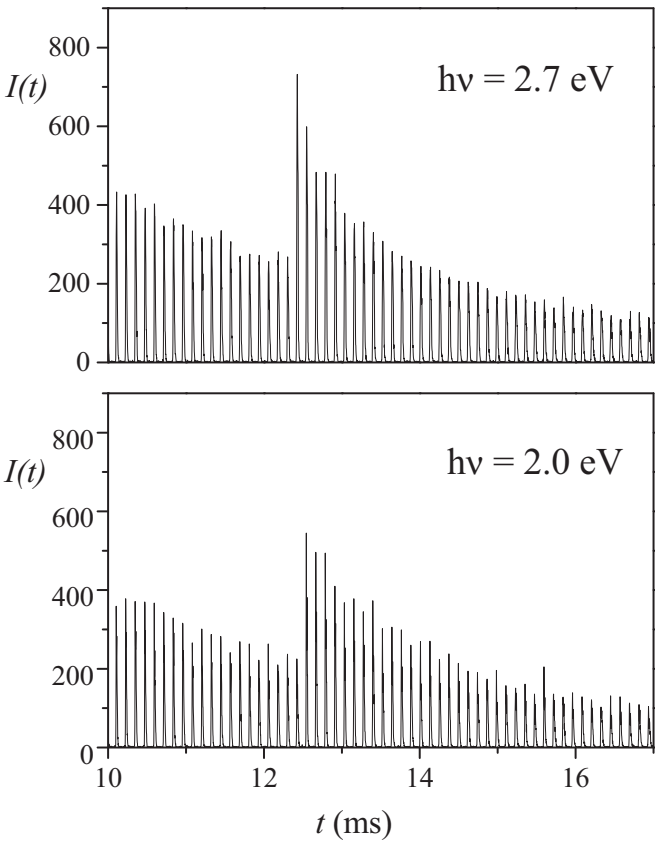

FIG. 3. Two spectra with photo-enhanced decays.

2.7 eV. Reference spectra without exposure to laser light were recorded under identical source and ring conditions, time-wise interleaving laser-on and laser-off spectra. The ion source was found to be very stable, with reproducible spontaneous decay rates as a function of time, with variations restricted to minor and slow fluctuations in the absolute overall ion intensity. Such source intensity variations were accounted for by a normalization using prelaser time counts of the laser-on and the laser-off spectra. The spontaneous decay showed no variation with respect to the exponential cutoff caused by the radiative cooling, and the decay rate as a function of time was in good agreement with the rates previously observed from a plasma source [12].

The main result of the experiments were the backshifted times of the photoinduced decays. As illustrated with a couple of examples in Ref. [6], the photon enhanced signal can be represented well by the expression

$$R_p(t) \propto \frac{1}{t - t_{las} + t_0}, \tag{17}$$

where t is the time after production of the ions in the source, t_{las} is the laser firing time, and t_0 the backshifted time. This simple expression only works for situations where, like here, the backshifted time is located in the pure power-law sector before radiative cooling modifies the decay. Irrespective of in which sector the backshifted time is located, its interpretation is the same, viz., as the reciprocal of the rate constant of the molecule at the energy $E(t_{las}) + h\nu$, modified with k_p as given above.

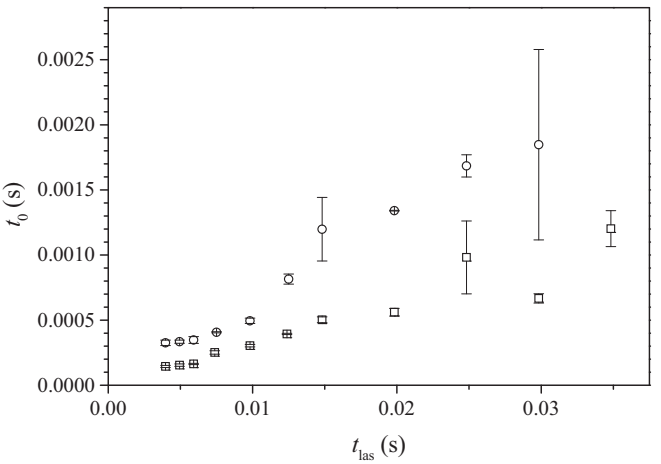

FIG. 4. Traces of t_0 as a function of laser firing time measured with the photon energies $h\nu = 2.0$ eV (circles) and 2.7 eV (squares). The error bars are statistical. Some amount of fluctuation beyond statistical are present, due to the so-called betatron oscillations, a well-known phenomenon from ion storage rings.

Figure 4 shows examples of the fitted t_0 for experiments with two different photon energies and a range of different laser firing times.

IV. DATA ANALYSIS

The data analysis proceeds from the data set comprising associated values of laser firing times t_{las}, backshifted times t_0, and photon energies $h\nu$ together with the rate constants for these times, $k(E(t))$, derived from the measured decay rates, as explained above.

The first part of the analysis is initiated by assigning a zero energy arbitrarily to the edge energy $E(t_{las})$ at some given laser time. In this case it was chosen to be $t_{las} = 0.00994$ s. A few alternative starting points were tried without any significant change in the result. The rates at both this time and after absorption of a photon are known, as is the difference in energy. This places all rates measured with the same laser firing time on the energy axis with known relative positions. Such data for different laser firing times are linked to each other when the different t_0s are close, ideally identical, for different laser firing times and photon energies. The criterion for two t_0s being identical was chosen to be a difference of no more than 10% in value. The computational procedure is illustrated in Fig. 5. All 62 measured combinations of laser firing times and photon energies were linked to the common energy reference this way. The linked energies are independent of the values of k_p, but the rate constants for each time are not. They need to be calculated with Eq. (11).

As the value of k_p is not known at this point, curves of the thermionic emission rate constant $k(E)$ were calculated for different assumed values of k_p, varying it from 10 to 100 s^{-1} in steps of 10 s^{-1}. For each of these, the logarithmic slope was fitted. The logarithmic slope takes the form

$$\frac{d\ln k}{dE} = \frac{\phi C_v}{E^2} = \frac{\ln(\omega/\bar{k})^2}{\phi C_v}, \tag{18}$$

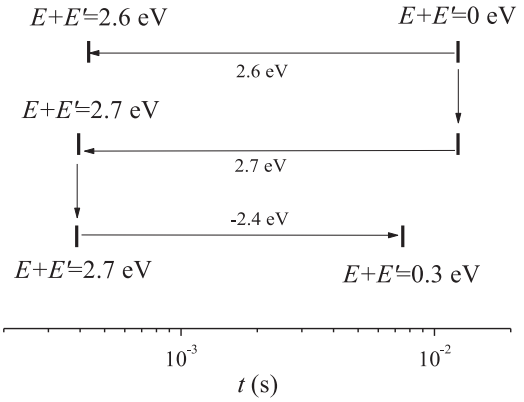

FIG. 5. The computational flow in the calculation linking the relative energies, illustrated with three laser firing times, two of which are identical. The energy assignment begins at the top right corner by choosing this as the zero of energy and flows in the direction of the arrows. The points at times around 10 ms correspond to data at t_{las}, and those at a few hundred μs are data at the corresponding t_0s. As described in the main text, all points can be assigned a known rate constant, modulo the value of k_p.

where $\bar{k}$ is the logarithmic midpoint of the data range for which the derivative is fitted.

The second step in the analysis is taken by considering the variation of the rate constants when the laser time is changed and the photon energy is kept constant. Taking the ratio of the rate constant at the backshifted time to the rate constant at the laser firing time one gets, with E_{las} denoting the energy edge at the laser firing time and using the expression for the energy resolved rate constant in Eq. (4),

$$\frac{k(t_0)}{k(t_{las})} = \exp\left(-\frac{\phi C_v}{E_{las}+h\nu}+\frac{\phi C_v}{E_{las}}\right) \approx \exp\left(\frac{\phi C_v h\nu}{E_{las}^2}-\frac{\phi (h\nu)^2}{E_{las}^3}\right), \tag{19}$$

or

$$\ln\left(\frac{k(t_0)}{k(t_{las})}\right) \approx \frac{\phi C_v h\nu}{E_{las}^2}\left(1-\frac{h\nu}{E_{las}}\right). \tag{20}$$

The left-hand side of this expression is expressed with the relations between rate constant and time in Eqs. (15) and (16). The value of E_{las} can be expressed in terms of the rate constant as

$$k(t_{las}) = \omega \exp\left(-\frac{\phi C_v}{E_{las}}\right) \Rightarrow E_{las} = \frac{\phi C_v}{\ln(\omega/k(t_{las}))}. \tag{21}$$

Inserting this and taking the square root gives the quasilinear relation

$$\left[\ln\left(\frac{k(t_0)}{k(t_{las})}\right)\right]^{1/2} = \left(\frac{h\nu}{\phi C_v}\right)^{1/2}[\ln(\omega t_{\rm ref}) - \ln(k(t_{las})t_{\rm ref})]\left(1-\frac{h\nu\ln(\omega/k(t_{las}))}{\phi C_v}\right)^{1/2}, \tag{22}$$

where $t_{\rm ref}$ is a reference time that can conveniently be taken as 1 s.

Repeating this procedure with t_{las} replaced by t_0 on the right-hand side gives a similar result apart from the exchange $t_{las} \to t_0$, and a change of sign on the last term in the last bracket. Averaging the two and dividing by $\sqrt{h\nu}$ gives

$$\frac{1}{\sqrt{h\nu}}\left[\ln\left(\frac{k(t_0)}{k(t_{las})}\right)\right]^{1/2} \approx \left(\frac{1}{\phi C_v}\right)^{1/2}\left[\ln(\omega t_{\rm ref}) - \frac{1}{2}\ln\left(k(t_{las})k(t_0)t_{\rm ref}^2\right)\right]. \tag{23}$$

When evaluating the quality of this approximation, it was compared with that of the ratio of rate constants expressed as

$$\ln\left(\frac{k(t_0)}{k(t_{las})}\right) = -\frac{\phi C_v}{E_{las}+h\nu}+\frac{\phi C_v}{E_{las}} = \frac{\phi C_v h\nu}{E_{las}(E_{las}+h\nu)} = \frac{h\nu}{\phi C_v}\ln\left(\frac{\omega}{k(t_0)}\right)\ln\left(\frac{\omega}{k(t_{las})}\right). \tag{24}$$

This is inconvenient for graphical representation, but a test using it (not shown) confirms the validity of the above approximation.

Equation (23) defines a straight line. The value of k_p enters into the values of $k(t_0)$ and $k(t_{las})$ and hence also of the slope and the intercept of the straight line. The intercept squared allows a comparison with the value obtained with Eq. (18) after a correction for the difference between timescales used in the factor $\ln(\omega t)$ in the two equations. The comparison of the two values is shown in Fig. 6 vs k_p. Consistency requires identical values for the two curves, yielding the value $k_p = 60\ {\rm s}^{-1}$. This value inserted into Eq. (23) gives the line in Fig. 7.

Another possible contribution to the analysis shown in Fig. 7 should be mentioned. It is obtained by replacing the rate constant at the laser firing time with one for a different photon energy, i.e., using two different photon energies and hence two

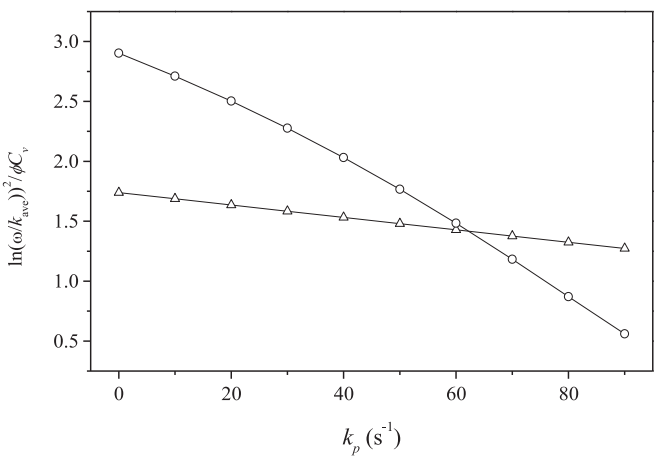

FIG. 6. The values of $\ln(\omega \times 1\ {\rm s})^2/\phi C_v$ vs k_p calculated with Eq. (18) (circles) and Eq. (23) (triangles).

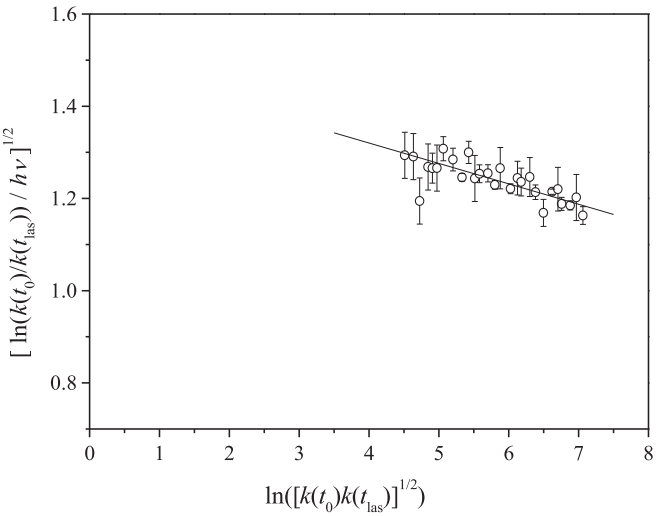

FIG. 7. Plot of the data calculated with Eq. (23) and $k_p = 60\ \mathrm{s}^{-1}$. The points are grouped in bunches 0.1 wide and the error bars are calculated as the statistical average of the mean. For a few points where there is only one datum in the bunch, the error is set to 0.05.

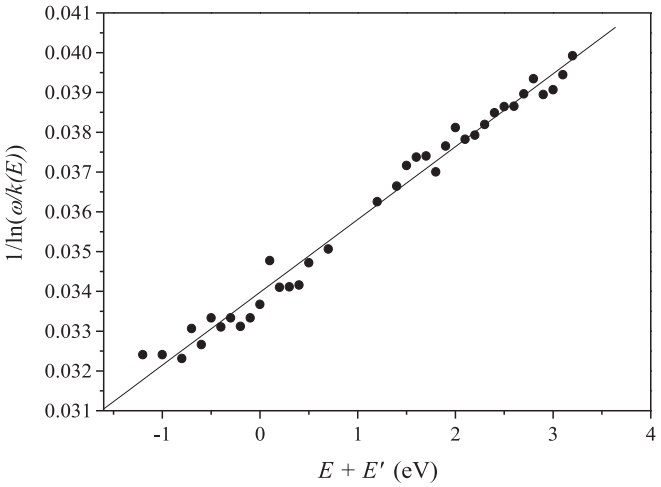

FIG. 8. Plot of Eq. (27) with rate constants calculated with the linking procedure explained in the main text, and the value $k_p = 60\ \mathrm{s}^{-1}$. The line is a straight line fit. The parameters of the line give the values $\phi C_v = 546 \pm 12$ eV and $E' = 18.6 \pm 0.4$ eV. The error in ω is not included in these two standard deviations.

different backshifted times from the same laser firing time. The equation then reads

$$\frac{1}{\sqrt{h\nu_1 - h\nu_2}}\left[\ln\left(\frac{k(t_0(1))}{k(t_0(2))}\right)\right]^{1/2} \approx \left(\frac{1}{\phi C_v}\right)^{1/2}\left[\ln(\omega t_{\mathrm{ref}}) - \frac{1}{2}\ln\left(k(t_0(1))k(t_0(2))t_{\mathrm{ref}}^2\right)\right], \tag{25}$$

where the arguments (1) and (2) refer to different photon energies at the same laser firing time. The present data (not shown) are too scattered to provide any strong confirmation of the analysis, but are consistent with it.

The parameters of the line in Fig. 7 gives the values

$$\ln(\omega\ 1\mathrm{s}) = 33.8 \pm 6.0, \quad \phi C_v = 510 \pm 180\ \mathrm{eV}, \tag{26}$$

corresponding to a frequency factor of $\omega = 4.9 \times 10^{14}\ \mathrm{s}^{-1}$ with a 1σ uncertainty of a factor 400.

The above results can be used to verify the procedure by applying them to the rate constants found with the linking procedure illustrated in Fig. 5. As k_p is known, also these rate constants are known, apart from the offset in energy. The expression for the rate constant is rewritten, reintroducing the offset energy E', as

$$\frac{1}{\ln(\omega/k(E))} = \frac{E + E'}{\phi C_v}. \tag{27}$$

Using the value of ω fitted above, the left-hand side is plotted vs E in Fig. 8. The expected straight line behavior is observed, and the fitted value of ϕC_v is consistent with the previously fit values, although the uncertainty is significant larger than the fit value indicates. The rate constant calculated with the two fit parameters from Fig. 8 and the previously determined ω from Eq. (26) is shown in Fig. 9. Also shown are the measured rate constants from Eqs. (11), calculated with the large photon energy parameter value $k_p = 60\ \mathrm{s}^{-1}$, the experimentally measured rates $R(t)$ and the fit values of the energies based on the measured values of t_0, as described in detail above.

V. DISCUSSION

The analysis has been based on experimental data and the result in Fig. 9 gives the rate constant from experimental data alone. The different determinations of the parameters can be summarized as a value for the frequency factor of $\omega = 5 \times 10^{14}\ \mathrm{s}^{-1}$ with an uncertainty of a factor 400; two values of ϕC_v of which 510 ± 180 eV must be considered the primary. The second value is consistent with this number but is derived assuming the above value of the frequency factor. Finally, the

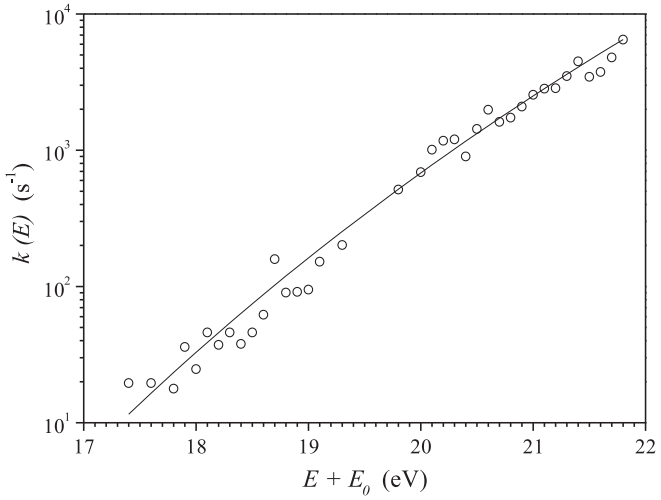

FIG. 9. The thermionic rate constant of C_{60}^- vs energy. Error bars can be taken as the average point-to-point fluctuation. The full line are the values calculated with the parameters $\omega = 4.9 \times 10^{14}\ \mathrm{s}^{-1}$, $\phi C_v = 546$ eV, and $E' = 18.6$ eV. The latter is added to the energy. As it includes the offset in the caloric curves, this is added as E_0.

zero of energy has been fitted to a value of 18.6 eV. The first two parameters in this list have obvious interpretations, but the energy offset also contains information about the reacting species.

The parameters extracted from the fits differ from the values that can potentially be measured in other experiments because approximating a microcanonical rate constant, which is essentially approximating a ratio of level densities with an exponential, will generate some finite-size corrections. These corrections were calculated in Ref. [23]. To leading order in the reciprocal heat capacity they can be summarized as

$$C_v = \bar{s} - \frac{\ln(\omega t)^2}{12\bar{s}}, \tag{28}$$

$$\phi = E_a + E_r - E_t, \tag{29}$$

where $\bar{s}$ is the average of the number of thermally activated oscillators of precursor and product, and the two energies E_r, E_t are the offsets in the canonical caloric curves for the anion (E_r) and the neutral molecule (E_t), defined as

$$E = s_i T - E_i, \tag{30}$$

where i represents either r or t and s_r, s_t are the s values for the reactant (the anion) and the transition state (the neutral) as indicated by the subscripts. E_a is the adiabatic electron affinity with the previously cited value of 2.67 or 2.68 eV.

The correction to the heat capacity is very minor for C_{60}, on the order on 1 in the units of k_B used, and can be ignored here. Also, the slight variation in the heat capacity due to its temperature dependence will be ignored (see the Appendix for a discussion of this question).

The correction to the activation energy is the most important. It vanishes for a harmonic-oscillator system if the number and frequencies are identical in the precursor and product because, for harmonic oscillators, the offsets are just the sum of their zero-point energies. Although the number of oscillators is identical for the anion and the neutral molecule and the oscillators can be considered harmonic because the degree of excitation is very low, a correction arises because the frequencies differ.

The entire sets of frequencies of the neutral and the anion are not known. The two anion infrared-active modes reported in Ref. [24] of 570 and 1374 cm^{-1} are shifted slightly relative to the neutral values of 570 and 1411 cm^{-1} [25]. If the reduction of the highest frequency is used as the scaling for all frequencies, the corresponding reduction in total zero-point energy of the anion compared with the neutral is 0.26 eV. For this estimate the set of vibrational frequencies of Ref. [26] was used. Although these frequencies refer to fullerite and not to gas-phase molecules, the values should be sufficiently precise for this purpose. The net result is to reduce the effective activation by 10%. At the same time the reduced vibrational quantum energies push the heat capacity up toward the classical canonical limit of $3N - 6$. The combined effect is therefore less than the 10% reduction of the activation energy alone. As the anion vibrational spectrum is by and large unknown, a more accurate estimate of the expected value of ϕC_v will not be attempted.

In the definition of an emission temperature which is used here, some offsets enter the energy content of the decaying anions [23]. To a sufficient precision the emission temperature is, in terms of the physical excitation energy E equal to

$$T_e = \frac{1}{C_v}\left(E - \frac{E_a}{2} + E_r\right). \tag{31}$$

The quantity in the bracket is the energy that appears on the abscissa in Fig. 9, i.e., the offset energy E_0 is equal to $E_r - E_a/2$. With the reduced frequencies for the anion, this amounts to $E_0 = 7.7$ eV. To get the physical energy on the abscissa in Fig. 9 this number therefore needs to be subtracted. The rate constant has consequently been determined for the range of energies 9.7 to 14.1 eV.

The frequency factor in the simplified expression for the rate constant used here can be calculated from the exact value determined by the expressions given in Ref. [1] with some correction factors which can be found in Ref. [23]. It is not an observable that can be compared with other measurable quantities, and as a calculation of it involves a number of factors with each their uncertainty, a calculation of its value will not be attempted here.

Finally, it is worthwhile to consider the amount of radiative cooling by low- and high-energy photon emission. The distinction between these two categories is made according to whether the emission of one photon quenches the electron emission channel. The large photon energies are defined as [11]

$$\frac{d\ln k}{dE}h\nu > 1 \Rightarrow h\nu > \frac{\phi C_v}{[\ln(\omega/\bar{k})]^2}w = \frac{510\,\text{eV}}{\ln(4.9\times 10^{14}/400)^2} = 0.66\,\text{eV}. \tag{32}$$

Photons of this magnitude are within thermal reach, as can be seen by a calculation of the microcanonical temperature. For the anion this is $(E + E_0 + E_a/2)/160$, where $E + E_0$ is the fitted effective energy content, and $E_a/2$ is the correction for the finite heat bath, which can be ignored for photon emission. The value of 160 is the heat capacity. This is slightly less than the contribution from all oscillators, which is 174 in the harmonic and high-temperature limit. The calculated effective temperature is then 0.12 eV for the typical energy of 18 eV. The phase space of the photon and the quadratic absorption cross section [7] makes the total emission rate proportional to the fourth power of the photon energy. In terms of the microcanonical temperature:

$$k_{\text{photon}}(h\nu)dh\nu \propto (h\nu)^4\frac{e^{-h\nu/T}}{1-e^{h\nu/T}}dh\nu. \tag{33}$$

The total emitted power is bounded from below by $0.66\,\text{eV}\times 60\,\text{s}^{-1} = 40\,\text{eV/s}$. This should be compared with the radiative energy loss of approximately 100 eV/s reported in Ref. [6]. As mentioned, this emitted power refers to the radiation emitted as continuous cooling exclusively. We can use this value to normalize Eq. (33) and find the total emitted power as well as the distribution on low- and high-energy photons. Using the photon energies up to 0.66 eV, the low-energy photon cooling determines the constant c as

$$100\,\text{eV/s} = c\int_0^{0.66\ \text{eV}}(h\nu)^5\frac{e^{-h\nu/T}}{1-e^{-h\nu/T}}dh\nu. \tag{34}$$

The corresponding high photon energy emission rate constant is

$$k_p = c \int_{0.66\,\mathrm{eV}}^{\infty} (h\nu)^4 \frac{e^{-h\nu/T}}{1 - e^{-h\nu/T}} dh\nu. \tag{35}$$

The value is calculated to be 120 s^{-1}, i.e., a factor of two higher than the fitted value. The value decreases to 90 s^{-1} for the temperature 0.11 eV. Considering that the spectrum in Eq. (33) is somewhat schematic, the agreement is reasonable. In any case, the data suggest that a considerable fraction of the radiative energy is emitted as high-energy photons. This is remarkable, both because the systems is as large as it is and because the electron affinity, which acts as the activation energy and therefore sets the temperature scale, is not particularly large compared with activation energies for unimolecular fragmentation, for example.

VI. SUMMARY AND PERSPECTIVES

The rate constant for thermal electron emission from C_{60}^- has been determined over a 4 eV energy range. The determination applies a simplified rate constant but does not rely on any modeling. The experimental input is the set of associated values of backshifted times, photon energies, and laser-firing times in a reheating experiment. The experiment was performed in a storage ring, which is an ion storage device which allows us to probe a wide range of times and thereby to cover a reasonable internal energy range.

The analysis provided the absolute value and the logarithmic derivative of the rate constant with respect to energy, and the product of activation energy and heat capacity, together with the frequency factor for the rate constant. The values were found to be in the range of expected and physically reasonable, although the uncertainties were not negligible. The main problem of the analysis of the present data is the presence of betatron oscillations. Although these are inherent to the operation of storage rings, their magnitude decreases in smaller rings, for simple geometrical reasons related to relative detector size [27]. The analysis presented here is a proof of principle for the method which provides rate constants for large systems that are otherwise in practice beyond reach of experimental measurement, and the commissioning of still smaller storage rings promise the possibility for still more accurate measurements. Other problems may arise with a reduction of the betatron oscillations. Application of the method to smaller molecules or clusters could require that finite heat capacities are taken into account. A deviation from the straight line behavior seen in Fig. 10 indicate that the finite heat capacity imposes modifications on the analysis. Such effects have been seen, e.g., in Ref. [28] for SF_6^-. Because the method described in this work is most urgently needed for large systems where heat capacities tend to vary smoothly with energy over the measured range, such complications are not expected to constitute a major drawback. Another limitation associated with level densities and thermal properties should be mentioned, viz. the possibility of a liquid-solid phase transition or, more correctly, the finite-size equivalent of this. This will modify the power-law decay as described in Ref. [3], essentially with an increase, in contrast with the decrease induced by radiative cooling, and is therefore directly observable in the measured spectra of spontaneous decays.

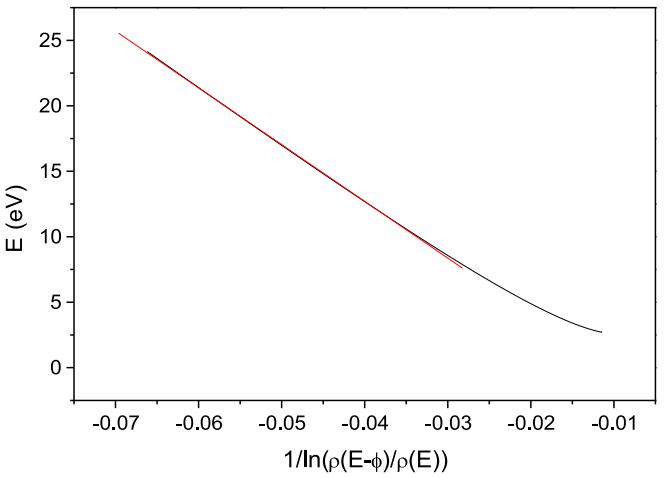

FIG. 10. The test of the approximation of the rate constant by the expression in Eq. (A1).

ACKNOWLEDGMENTS

A. E. K. Sundén, M. Goto, J. Matsumoto, H. Shiromaru, H. Tanuma, T. Azuma, J. U. Andersen, and S. E. Canton [6] are gratefully acknowledged for the productive collaboration that provided the experimental material of this paper.

APPENDIX: THE APPROXIMATION OF THE RATE CONSTANT

The use of Eq. (4) requires that parameters extracted from the experiments must be corrected before they can be compared with parameter values from other types of experiments. The corrections are known [23] and have been applied in the Discussion section.

The energy in the denominator, $E + E'$, is the sum of the true thermal energy E and an offset E', which is required to account for situations where the thermal energy is not simply proportional to the temperature. The offset includes the zero-point energy of the harmonic oscillators, which provide the largest part of the heat capacity of the molecule, but also accommodates any other thermal offset that may be present below E, for whatever reasons.

The main energy dependence of the electron-emission rate constant is the contribution from the ratio of level densities, ρ, and the main question therefore concerns the accuracy of the approximation

$$\frac{\rho(E - \phi)}{\rho(E)} = \exp\left(-\frac{\phi C_v}{E + E'}\right). \tag{A1}$$

The quality of this approximation is best seen by plotting E vs $\ln(\rho(E - \phi)/\rho(E))$. For this purpose the known electron affinity and the known frequencies of the molecule in combination with the Beyer-Swinehart algorithm are used. From the rewritten relation

$$E = \frac{\phi C_v}{\ln\left(\frac{\rho(E-\phi)}{\rho(E)}\right)} - E', \tag{A2}$$

a straight line is expected. It is indeed also seen in Fig. 10. The slope is 434 eV and the offset gives $E' = 4.64$ eV, both in good agreement with the expected values. Importantly, the line is straight to a good approximation. The value where the expected abscissa is located is centered slightly below -0.04, with an ± 2 eV range at each sides on the ordinate. This is well in the linear part of the curve.

[1] J. U. Andersen, E. Bonderup, and K. Hansen, J. Phys. B: At. Mol. Phys. **35**, R1 (2002).

[2] K. Hansen, J. U. Andersen, P. Hvelplund, S. P. Møller, U. V. Pedersen, and V. V. Petrunin, Phys. Rev. Lett. **87**, 123401 (2001).

[3] K. Hansen, Mass Spectrom. Rev. (2020), doi: 10.1002/mas.21630.

[4] S. Matt, O. Echt, T. Rauth, B. Dünser, M. Lezius, A. Stamatovic, P. Scheier, and T. D. Märk, Z. Phys. D: At., Mol. Clusters **40**, 389 (1997).

[5] S. Matt, P. Scheier, A. Stamatovic, H. Deutsch, K. Becker, and T. D. Märk, Philos. Trans. R. Soc., A **357**, 1201 (1999).

[6] A. E. K. Sundén, M. Goto, J. Matsumoto, H. Shiromaru, H. Tanuma, T. Azuma, J. U. Andersen, S. E. Canton, and K. Hansen, Phys. Rev. Lett. **103**, 143001 (2009).

[7] J. Andersen and E. Bonderup, Eur. Phys. J. D **11**, 413 (2000).

[8] J. U. Andersen, E. Bonderup, and K. Hansen, J. Chem. Phys. **114**, 6518 (2001).

[9] C. Brink, L. H. Andersen, P. Hvelplund, D. Mathur, and J. D. Voldstad, Chem. Phys. Lett. **233**, 52 (1995).

[10] D.-L. Huang, P. D. Dau, H.-T. Liu, and L.-S. Wang, J. Chem. Phys. **140**, 224315 (2014).

[11] P. Ferrari, E. Janssens, P. Lievens, and K. Hansen, Int. Rev. Phys. Chem. **38**, 405 (2019).

[12] J. U. Andersen, C. Brink, P. Hvelplund, M. O. Larsson, B. Bech Nielsen, and H. Shen, Phys. Rev. Lett. **77**, 3991 (1996).

[13] K. Hansen and E. Campbell, J. Chem. Phys. **104**, 5012 (1996).

[14] C. G. Granqvist, R. A. Buhrman, J. Wyns, and A. J. Sievers, Phys. Rev. Lett. **37**, 625 (1976).

[15] Y. H. Kim and D. B.Tanner, Phys. Rev. B **39**, 3585 (1989).

[16] K. Hansen, Int. J. Mass Spectrom. **430**, 14 (2018).

[17] S. P. Møller, Nucl. Instrum. Methods Phys. Res., Sect. A **394**, 281 (1997).

[18] S. Jinno, T. Takao, Y. Omata, A. Satou, H. Tanuma, T. Azuma, H. Shiromaru, K. Okuno, N. Kobayashi, and I. Watanabe, Nucl. Instrum. Methods Phys. Res., Sect. A **532**, 477 (2004).

[19] L. H. Andersen, O. Heber, and D. Zajfman, J. Phys. B: At., Mol. Opt. Phys. **37**, 57 (2004).

[20] S. Martin, J. Bernard, R. Brédy, B. Concina, C. Joblin, M. Ji, C. Ortega, and L. Chen, Phys. Rev. Lett. **110**, 063003 (2013).

[21] H. T. Schmidt, R. D. Thomas, M. Gatchell, S. Rosén, P. Reinhed, P. Löfgren, L. Brännholm, M. Blom, M. Björkhage, E. Bäckström *et al.*, Rev. Sci. Instrum. **84**, 055115 (2013).

[22] Y. Nakano, Y. Enomoto, T. Masunaga, S. Menk, P. Bertier, and T. Azuma, Rev. Sci. Instrum. **88**, 033110 (2017).

[23] K. Hansen, Chem. Phys. Lett. **620**, 43 (2015).

[24] P. Kupser, J. D. Steill, J. Oomens, G. Meijer, and G. von Helden, Phys. Chem. Chem. Phys. **10**, 6862 (2008).

[25] L. Nemes, R. S. Ram, P. F. Bernath, F. A. Tinker, M. C. Zumwalt, L. D. Lamb, and D. R. Huffman, Chem. Phys. Lett. **218**, 295 (1994).

[26] J. Menéndez and J. B. Page, Vibrational Spectroscopy of C_{60}, *Light Scattering in Solids* (Springer, Berlin, 2000), Vol. VIII, pp. 27–95.

[27] J. Matsumoto, R. Saiba, K. Gouda, E. Makino, K. Hashimoto, K. Fueta, N. Kondo, and H. Shiromaru, Nucl. Instrum. Methods Phys. Res., Sect. B **454**, 23 (2019).

[28] S. Menk, S. Das, K. Blaum, M. W. Froese, M. Lange, M. Mukherjee, R. Repnow, D. Schwalm, R. von Hahn, and A. Wolf, Phys. Rev. A **89**, 022502 (2014).